JOURNAL OF Applied Polymer SCIENCE

# Effect of the exposure time on the structure and performance of hydrophobic polydimethylsiloxane–poly(vinylidene fluoride) membranes via a non-solvent-induced phase separation process in a clean room

**Heiyan Zhang,[1] Bingbing Li,[1] De Sun,[1] Dayong Li,[2] Jing Li,[1] Xiaofeng Shao[1]**

[1]Department of Chemical Engineering, Changchun University of Technology, 2055 Yanan Street, Changchun 130012, People's Republic of China

[2]COFCO Biochemical Energy (Yushu) Company, Limited, Economic Development Wukeshu, 1 Dongfeng Street, Changchun 130033, People's Republic of China

Correspondence to: D. Sun (E-mail: sunde2002@126.com)

**ABSTRACT:** The objective of this study was to investigate the effects of the exposure time on the properties and permeability of polydimethylsiloxane (PDMS)–poly(vinylidene fluoride) (PVDF) blend hydrophobic microporous membranes, which were fabricated via a non-solvent-induced phase separation process at 25 °C and 60% relative humidity in a clean-room circumstance. For the prepared PDMS–PVDF membranes, the membrane morphologies were observed by scanning electron microscopy. Crystalline structures were observed by X-ray diffraction. Pore structures were analyzed by membrane porosity and mean pore size. Hydrophobicity was measured by contact angle measurement, and the mechanical properties were characterized by tensile strength testing. Our study results show that with increasing exposure time from 10 to 110 s, all of the membranes showed a similar pore structure: a spongelike substrate layer with a thin realm of fingerlike structures under the top surface. Phase separation between PDMS and PVDF occurred. The membrane porosity and mean pore radius decreased, and the membrane thickness increased. The membrane hydrophobicity decreased, and the mechanical properties first increased and then decreased. In addition, vacuum membrane distillation experiments were conducted. With the increase in the exposure time from 10 to 110 s, the membrane permeate flux decreased from 16.54 to 6.65 kg $m^{-2}{\cdot}h^{-1}$, and the salt rejection was higher than 99.9%. © 2016 Wiley Periodicals, Inc. J. Appl. Polym. Sci. **2016**, *133*, 43842.

**KEYWORDS:** membranes; phase behavior; properties and characterization; separation techniques

Received 5 January 2016; accepted 26 April 2016
**DOI: 10.1002/app.43842**

## INTRODUCTION

Membrane distillation (MD), a new separation technology with the advantages of low energy consumption and high productivity, could play an increasingly important role in industry and our daily life.[1] There are a variety of MD processes, and the most popular ones are direct-contact membrane distillation (DCMD), vacuum membrane distillation (VMD), sweeping gas MD, and air-gap membrane distillation (AGMD).[2] Table I summarizes recent studies related to MD from 2010 to 2016. Generally, VMD has a higher permeation flux and less conductive heat loss compared to other MD forms.[23] In a VMD process, a membrane is applied as a barrier to reject solute and prevent aqueous solution from penetrating into membrane pores; therefore, microporous membranes with excellent features in hydrophobicity, pore structure, and mechanical properties are very crucial.[21,24,25] Of all hydrophobic polymers, poly(vinylidene fluoride) (PVDF), polypropylene, polytetrafluorethylene (PTFE), and polyethylene (PE) are the most commonly used materials for the fabrication of the hydrophobic microporous membranes used in the VMD process.[8] Among these polymers, with excellent chemical, physical, and mechanical properties and outstanding thermal stability, PVDF has been widely used to produce microporous membranes for VMD processes.[21–28] For the fabrication of PVDF membranes, there are several different methods, such as the non-solvent-induced phase separation (NIPS) process,[29–31] thermally induced phase separation process,[32,33] and vapor-induced phase separation process.[24] Among these processes, NIPS is the mostly used for its flexibility in the selection of solvent and nonsolvent.[1,2]

In a NIPS process, a polymer casting solution was cast on a suitable support, and then, with the support, it was immersed in a nonsolvent bath for precipitation. During the precipitation, the polymer demixing rate and phase-separation patterns (liquid–liquid and liquid–solid) can affect the structure and

**Table I.** Recent Studies Related to MD from 2010 to 2016

| Reference | Polymer | Geometry | Year | Type | Flux (kg $m^{-2}$·$h^{-1}$) | Rejection | Feed |
|---|---|---|---|---|---|---|---|
| Tong *et al.*[3] | Hyflon AD60/PVDF | Hollow fiber | 2016 | VMD | 10 | >99.9% | 35 g/L NaCl |
| Zuo *et al.*[4] | PE | Flat sheet | 2016 | DCMD | 123 | >99.9% | 3.5 wt % NaCl |
| Chen *et al.*[5] | FEP | Hollow fiber | 2015 | VMD | 8.4 | >99.9% | 35 g/L NaCl |
| Lin *et al.*[6] | PVDF | Hollow fiber | 2015 | AGMD | 5.5 | >99.9% | 7.0 wt % NaCl |
| Kharraz *et al.*[7] | PVDF | Flat sheet | 2015 | DCMD | 18 | >99% | Seawater |
| Simone *et al.*[8] | PVDF | Hollow fiber | 2014 | VMD | 14.46 | >99.9% | Synthetic seawater |
| Devi *et al.*[9] | PVDF | Flat sheet | 2014 | VMD | 12 | >99% | 3–10 wt % NaCl |
| Shirazi *et al.*[10] | PTFE | Flat sheet | 2014 | DCMD | 48 | >99% | 3.5,4.5 wt % NaCl |
| Drioli *et al.*[2] | PVDF | Hollow fiber | 2013 | VMD and DCMD | 21.78–41.78 | — | Double distilled water |
| Fan *et al.*[11] | PVDF | Flat sheet | 2013 | VMD | 22.4 | >99.9% | 3.5 wt % NaCl |
| Sarbatly and Chiam[12] | PVDF | Flat sheet | 2013 | VMD | 9.28 | — | Geothermal water |
| Song and Jiang[13] | PVDF | Hollow fiber | 2013 | DCMD | 20 | >99.9% | 3 wt % NaCl |
| Essalhi *et al.*[14] | PVDF | Nanofiber | 2013 | DCMD | 13.7–15.2 | >99% | 0–60 g/L NaCl |
| Edwie *et al.*[15] | PVDF | Hollow fiber | 2012 | DCMD | 83.4 | >99.9% | 3.5 wt % NaCl |
| Tang *et al.*[16] | PVDF | Hollow fiber | 2012 | VMD and DCMD | 11–23 | >99.9% | 9.09 wt % NaCl |
| Fan and Peng[17] | PVDF | Hollow fiber | 2012 | VMD and DCMD | 18.9 and 22.4 | >99.8% | 35 g/L NaCl |
| Singh and Sirkar[18] | PTFE | Flat sheet | 2012 | DCMD | 195 | — | 1 wt % NaCl |
| Prince *et al.*[19] | PVDF–clay | Hollow fiber | 2012 | DCMD | 5.7 | >99% | 3.5 wt % NaCl |
| Wang *et al.*[20] | PVDF | Hollow fiber | 2011 | DCMD | 98.6 | >99.9% | 3.5 wt % NaCl |
| Teoh *et al.*[21] | PVDF/PTFE | Hollow fiber | 2011 | DCMD | 50.9 | >99.9% | 3.5 wt % NaCl |
| Simone *et al.*[22] | PVDF/PVP | Hollow fiber | 2010 | VMD | 3.5–18 | >99.9% | Simulating seawater |

FEP, poly(tetrafluoroethylene-*co*-hexafluoropropylene); Hyflon AD60, copolymer of tetrafluoroethylene and 2,2,4-trifluoro-5-trifluoromethoxy-1,3-dioxole.

**Table II.** Preparation Conditions for the PDMS–PVDF Membranes

| Membrane | PVDF/PVP/DMAc/TEP (mass ratio) | PDMS/PVDF (mass ratio) | THF/PDMS (mass ratio) | Exposure time (s) |
|---|---|---|---|---|
| MT1 | | | | 10 |
| MT2 | | | | 30 |
| MT3 | 12:3:34:51 | 1:5 | 10:1 | 50 |
| MT4 | | | | 70 |
| MT5 | | | | 90 |
| MT6 | | | | 110 |

properties of the microporous membranes.[21,25–28] The factors that may influence precipitation rate include the choice of polymer,[2,25] polymer concentration,[2,9,16] additives[2,21,26,27] in the casting solution, exposure time,[2,16,28] temperature,[16,23] composition of the coagulation bath,[8,22,23] immersion time,[2,23] and casting thickness of the polymer solution.[23] For the preparation of PVDF microporous membranes used for MD processes, the usual solvents used to dissolve PVDF include *N*,*N*-dimethylformamide,[2] *N*,*N*-dimethylacetamide (DMAc),[9,16,22,23] and *N*-methylpyrrolydone;[2,8,22,25] the additives include polyvinylpyrrolidone (PVP),[2,22] PTFE,[21,28] LiCl,[16] $CaCO_3$,[26] and $H_2O$,[27] and the usual coagulation baths include water, ethanol, and their mixtures.[8,23] The rapid precipitation rate of casing solution creates a fingerlike macrovoid structure, whereas the low precipitation rate creates a spongelike structure or spherulite formation. The spongelike structure is more favorable than the fingerlike structure for improvements in the membrane porosity and mechanical properties, which are important factors related to the MD performances.[21–28]

In recent years, an increasing number of researchers have investigated ways to improve the VMD performance of a PVDF microporous membrane fabricated via NIPS processes. Simone *et al.*[8] found that the properties of microporous hydrophobic hollow fibers were strongly influenced by the composition and flow rate of bore fluid. Figoli *et al.*[25] discovered that the polymer concentration played a major role in determining the final membrane morphology. Thomas *et al.*[23] used a two-stage coagulation bath system to prepare membranes that had a uniform and open structure on the surface and an asymmetric interconnected pore structure all through the thickness of the membranes. Tang *et al.*[16] obtained high-permeate flux membranes with LiCl and PEG-400 as nonsolvent additives to make polymer dopes. Drioli *et al.*[2] confirmed that the transmembrane flux was related to the spinning conditions and polymeric dope compositions. Studies of Devi *et al.*[9] showed that the membranes prepared with low-concentration polymer casting solutions were much more porous compared to those prepared with high-concentration polymer casting solutions. Chen *et al.*[34] fabricated microporous membranes with a blend of high-molecular-weight PVDF and low-molecular-weight PVDF and found that the water vapor flux was highest when the high-molecular-weight PVDF/low-molecular-weight PVDF ratio was 4:6. In addition, the influence of the exposure time on the properties of PVDF microporous membranes used for VMD have scarcely been reported.

In our previous work,[35] polydimethylsiloxane (PDMS)–PVDF blend hydrophobic microporous membranes for the desalination of VMD were fabricated via a NIPS process with tetrahydrofuran (THF), triethyl phosphate (TEP), and DMAc as the solvent and water as the nonsolvent. The influences of the PDMS/PVDF mass ratio on the membrane morphology, crystalline structure, pore structure, hydrophobicity, mechanical characteristics, and permeability were investigated. Compared with the fingerlike pore PVDF membrane, the PDMS–PVDF membranes exhibited both fingerlike and spongelike pore structures; in addition, PDMS–PVDF membranes had the bigger porosity, larger mean pore size, higher hydrophobicity, stronger mechanical properties, and better VMD performances. When the PDMS content in the casting solution increased, the PDMS polymer chains was evenly distributed among the PVDF polymer chains. When the mass ratio of PDMS/PVDF attained 1:3, phase separation occurred between the PDMS polymer and the PVDF polymer because of the excessive PDMS polymer chains.

In this study, on the basis of the results of our previously work, the effects of the exposure time on the morphology, hydrophobicity, and mechanical properties of the PDMS–PVDF membranes were investigated to further improve the VMD performance of the membranes; the correlations of the membrane properties and VMD performance were evaluated.

## EXPERIMENTAL

### Materials

PVDF (SOLEF 6020/1001) was purchased from Solvay Solexis, Inc. (France). PVP K30 (weight-average molecular weight = 3000) was produced by Tianjin Tiantai Fine Chemicals Co., Ltd. (China). PDMS (Silicone Rubber 107, weight-average molecular weight = 5000) was bought from Shanghai Resin Co. (China). DMAc, TEP, and THF were supplied by Sinopharm Chemical Reagent Co., Ltd. (China). Deionized water was self-produced in our laboratory. All of the chemicals used in this study were analytical grade and were used as received without further purification.

### Preparation of the Membranes

PDMS–PVDF flat microporous membranes were prepared via a NIPS process as described elsewhere.[35] The polymer powder was dried at 80 °C in a drying oven for 24 h. PVDF and PVP (pore-forming additives) were added to the organic solvent of mixed TEP and DMAc under mechanical stirring at 60 °C to form a PVDF solution. The solution then was put in a drying oven

overnight at 60 °C to ensure the complete dissolution of the polymers. PDMS was dissolved in THF by magnetic stirring for 2–3 h at room temperature, and then, the PDMS solution was added to the prepared PVDF solution at a mass ratio of 1:5 PDMS/PVDF. The mixed solution was mechanically stirred for 4 h at ambient temperature to obtain a homogeneous PDMS–PVDF casting solution. After vacuum deaeration, the casting solution was cast onto a glass plate at 25 °C and 60% relative humidity with a glass rod. The film was exposed in the air for different time periods in a clean-room circumstance, and together, with a glass plate, it was immersed into the coagulation bath (deionized water). Taken out from the coagulation bath, the precipitated film was peeled off and soaked in fresh deionized water for 4 days to remove the residues of the solvent. The deionized water was changed twice a day. The membranes were then dried in the air. The preparation conditions of the PDMS–PVDF membranes in this study are listed in Table II.

### Membrane Characterization

**Light Transmittance.** The phase-inversion kinetics of the casting solution could be simulated through a light transmittance experiment, which was based on the principle that demixing would lead the light transmittance to decrease. The light transmittance experiment was performed with a self-made device that was described in our previous report.[35] A collimated laser was directed onto the glass plate, which was immersed in a nonsolvent coagulation bath such as water, ethanol, or water–ethanol. The data of light intensity were captured by the light detector and were transferred to a computer. The precipitation rate of the casting solution were characterized by the curve of light transmittance versus the immersion time.

**Membrane Morphology.** The structures of the top surface, bottom surface, and cross section of the prepared flat membranes were observed by scanning electron microscopy (SEM; JSM-5600LV, Japan). To evaluate the skin layers, the enlarged SEM images near the top surfaces of the cross sections were observed by SEM (SUPRA 40, Carl Zeiss, Germany). The membrane samples were frozen in liquid nitrogen and were then broken to obtain a cross section. The samples were sputtered with gold by a sputter coater (KYKY SBC-12) and were then tested by SEM.

**Membrane Porosity.** The membrane porosity was defined as the total volume of the pores divided by the volume of the microporous membrane and was determined by gravimetric method. A sample of the wet membrane, which was soaked in a low-surface-tension (16 dyn/cm) wetting liquid (Profil, IB-FT GmbH, Germany), was weighed with a highly sensitive electronic balance (ALC-1100.2, Sartorius, Germany) with an accuracy of 0.0001 g. The thickness of the wet membrane was measured by an electronic digital caliper. The porosity was calculated with the following equation:

$$\text{Porosity} = (W_1 - W_2)/(A\delta_m\rho) \quad (1)$$

where $W_1$ is the weight of the wet membrane (g), $W_2$ is the weight of the dry membrane (g), $A$ is the area of the wet membrane, $\delta_m$ is the thickness of the wet membrane (cm), and $\rho$ is the Profil density (1.87 g/cm$^3$). In our experiments, for each membrane, three samples were tested to obtain an average value.

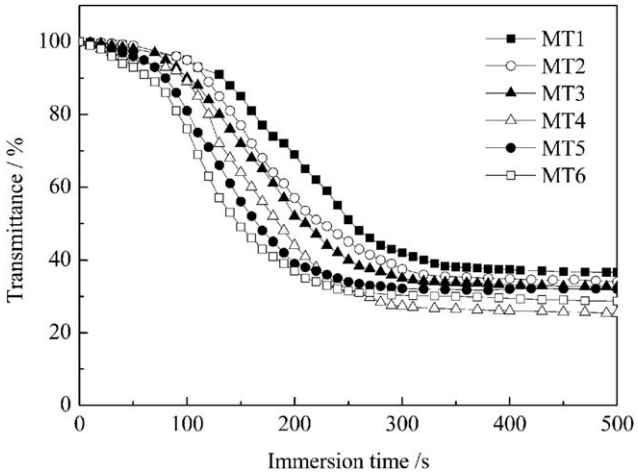


**Figure 1.** Precipitation rates of the PDMS–PVDF casting solutions with different exposure times.

**Mean Pore Size.** The mean pore size of the PDMS–PVDF membranes was investigated with a capillary flow porometer (Porolux, IB-FT GmbH, Germany) with a wet/dry flow method. The sample (effective membrane area = 2.7 cm$^2$) was wetted with Profil and was placed into a test cell, through which compressed air flowed, and then, the measurements were carried out according to a procedure described in the literature.[36] The mean pore size was determined with the aid of Porolux 500 software (porometer).

**X-ray Diffraction (XRD).** The XRD spectra of the PDMS, PVDF, and PDMS–PVDF membranes were obtained at room temperature with a D-MAX IIA X-ray diffractometer (Rigaku, Japan). The diffractograms were measured at a scanning speed of 10 °/min in the 2θ range 5–50 ° by means of a tube voltage of 40 kV and a tube current of 30 mA.

**Hydrophobicity.** The membrane hydrophobicity was characterized by the measurement of the contact angle between the membrane surface and water by a contact angle meter (DSA30, KRuss GmbH, Germany) with the sessile drop method. A water drop (2 μL) was carefully deposited on both the top and bottom surfaces; then, the image of the sessile drop was taken, and the contact angle value was measured from shape analysis. To obtain the average value, at least five locations were tested for one membrane sample.

**Mechanical Properties.** The mechanical properties of the membranes were determined by a tensile tester (Instron 3365) at a loading velocity of 20 mm/min and room temperature. At least five samples were tested to obtain an average value.

**VMD.** The VMD apparatus used in this case was as described as in the literature.[35] VMD experiments were conducted with a crossflow laboratory scale membrane unit with a relatively small effective membrane area of $4.6 \times 10^{-3}$ m$^2$. A 10-L feed tank was kept at 50 °C in a water bath controlled by a temperature controller. A solution of 20 g/L aqueous NaCl was used as the feed with a flow rate of 10 L/min as circulated by a circulation pump. The downstream vacuum pressure was 90 KPa, which controlled by a vacuum pump. After the operation reached a

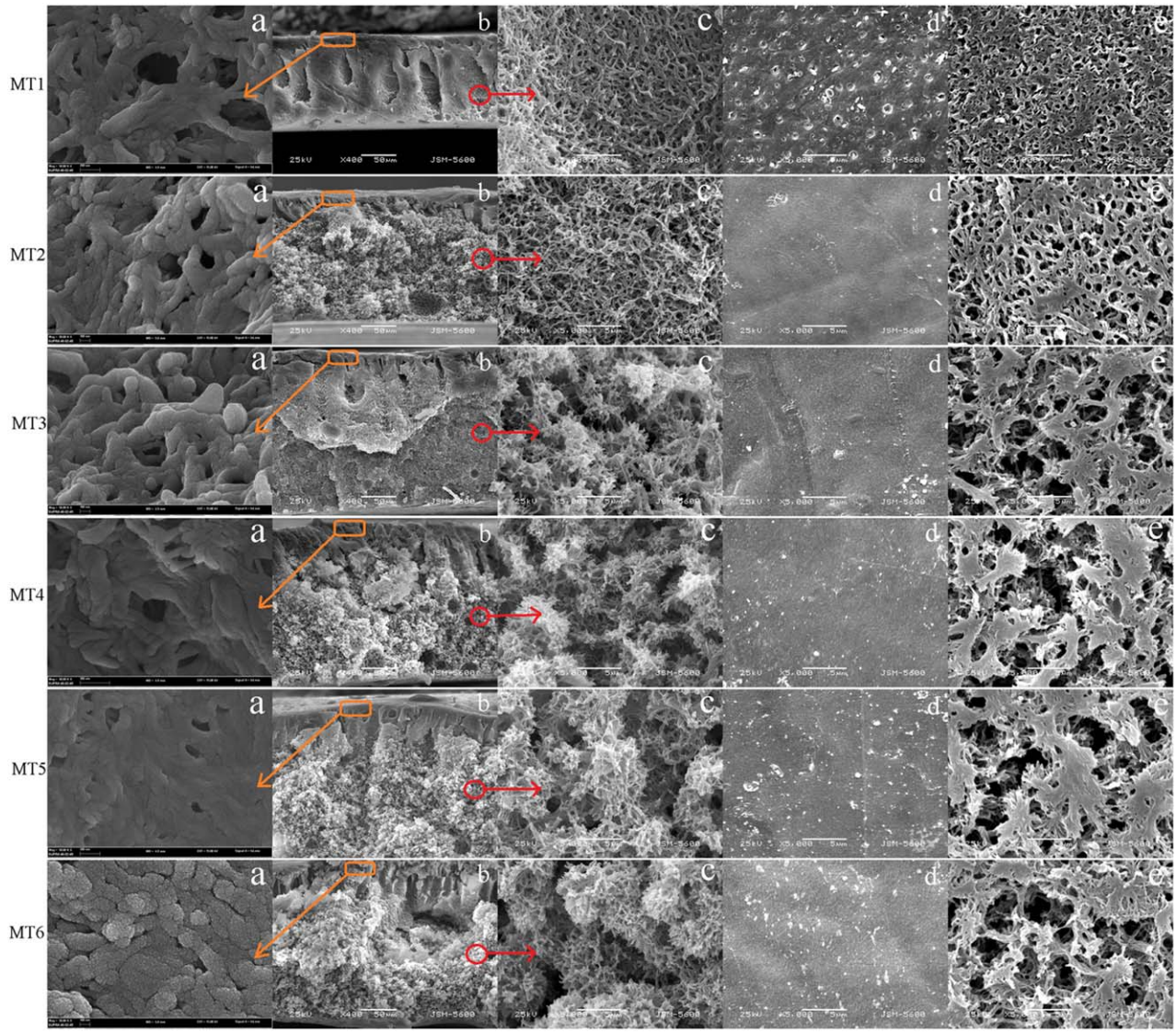


**Figure 2.** SEM images of the PDMS–PVDF membranes with different exposure times: (a) cross section near the top surface (magnification, 50,000×), (b) cross section (magnification, 400×), (c) cross section (magnification, 5000×), (d) top surface (magnification, 5000×), and (e) bottom surface (magnification, 5000×). [Color figure can be viewed in the online issue, which is available at wileyonlinelibrary.com.]

steady state (ca. 30 min after it was started), the permeate vapor was condensed in a chiller and was then collected in a filter flask. The NaCl concentration in the permeate solution was analyzed by a conductivity indicator. The calculation of the permeation flux and the rejection rate was performed as follows:

$$\text{Permeation flux } (\text{L m}^{-2} \cdot \text{h}^{-1}) = V/AT \quad (2)$$

$$\text{Rejection rate} = [1-(c_p/c_f)] \times 100\% \quad (3)$$

where $V$ is the permeation volume (L), $A$ is the effective membrane area, $T$ is the operation time (h), and $c_f$ and $c_p$ are the NaCl concentration (g/L) in the feed and permeate solution, respectively.

## RESULTS AND DISCUSSION

### Light Transmittance Measurement

Figure 1 demonstrates the precipitation kinetics of the casting solutions, which were prepared with the same dope solution but with different exposure times. When the exposure time increased from 10 to 110 s, all casting solutions presented the same delayed demixing process. The precipitation rate increased, the delay time was reduced from 150 to 80 s, and the time for the transmittance to reach a steady state was reduced from 340 to 250 s. A possible explanation for this could have been that during the exposure, with the evaporation of the solvent, the concentrations of PVDF, PDMS, and additives in the casting solution increased. Meanwhile, the polymer viscosity increased, so when the casting films were immersed into the harsh coagulation bath (water), the membrane precipitation time shortened. This was consistent with the description of Li *et al.*[38] The change in the precipitation rate, in turn, caused a change in the microporous structure of the membranes.

### Morphology

Figure 2 exhibits the morphologies of the whole cross section, top surface, bottom surface, and part of the cross sections near

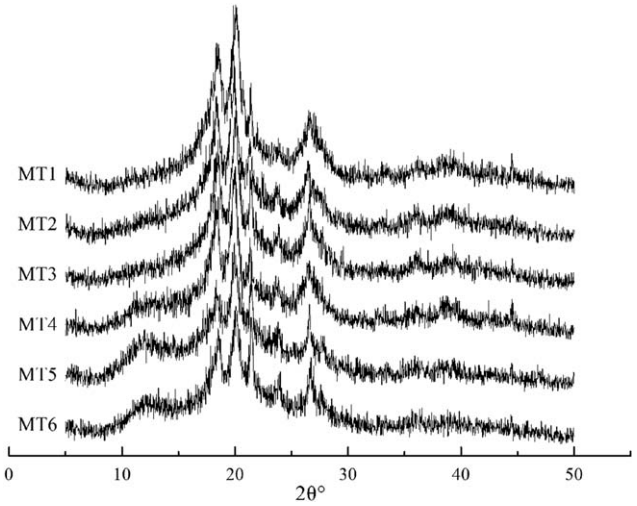


**Figure 3.** XRD patterns of the PDMS–PVDF membranes.

top surfaces of the PDMS–PVDF membranes, which were prepared with different exposure times. When the cross sections were magnified 400 times, all of the SEM images showed a similar pore structure: a spongelike substrate layer with a thin fingerlike realm under the top surface. In addition, there were some tear-shaped macrovoids only for MT1. When the cross sections near the top surfaces were magnified by 50,000×, with the increase of exposure time, the interspaces were near the top surface skin layers and decreased. However, when the cross sections were magnified by 5000×, there existed big differences. Networklike microstructures were observed on the cross sections of MT1 and MT2, whereas spherulitic microstructures were observed for MT3, MT4, MT5, and MT6. With increasing exposure time from 50 to 110 s, the diameter of the spherulitic microstructure grew, and the interspaces among the spherulitic microstructures got larger and larger. This result was very similar to that reported the literature, in which Peng *et al.*[24] prepared hydrophobic PVDF membranes via a vapor-induced phase separation method and found that with increasing exposure time, the cross section showed a spherulitic morphology. For the top surfaces, from the SEM images, round pores on the top surface of MT1 were found, whereas the other membranes showed dense top surfaces without pores. As the exposure time increased, white markings started to appear on the top surfaces of the membranes, and the number of the white markings increased. From the SEM images of the bottom surfaces, voids were observed; with increasing exposure time, the bottom surfaces became uneven, and the average size of the voids increased.

PVDF is a semicrystalline polymer. According to the pore-formation mechanism,[9,22,24,25] a fast precipitation will result in a liquid/liquid demixing; this can lead to an interconnected cellular-type structure, whereas low precipitation may result in solid/liquid demixing, which could cause a spherical globule-type structure. When the cast film was exposed to humid air, the solvents in the dope (DMAc + THF) evaporated, especially THF, which caused an increase in the polymer concentration in the casting film. With increasing exposure time, more solvent evaporated from the casting film; this induced the crystallization of the PVDF polymer in the coagulation bath.[2,9,16,28] From the cross-sectional pictures of MT1 to MT6, we observed that with increasing exposure time, demixing changed from liquid/liquid to solid/liquid, and the pore structure changed from cellular type to globule type. When the exposure time was 10 s, that is, when the polymer concentration was the lowest, droplet coalescence took place easily before the solidification of the polymer-rich phase, and this resulted in the large tear-drop macrovoids. This was in according with the literature.[25] When the exposure time increased from 30 to 110 s, which indicated an increase in polymer concentration in the films, the tear-drop macrovoids disappeared, and the cross section of the membranes turned into a spongelike structure. For the top and bottom surfaces, according to the macrovoid formation mechanism,[9] the lower concentration of the dope solution was more favorable for pore initiation than the higher concentration of the dope solution. So in this study, from MT1 to MT6, as the concentration of casting solution increased, for the bottom surfaces, the pore size increased, and the surfaces became uneven. For the top surfaces, cellular pores appeared on the top surface of the MT1 because it had the lowest polymer concentration of all the casting films, but for MT2 to MT6, the longer exposure caused a higher polymer concentration of casting films and resulted in the dense surfaces.[2] In addition, because THF evaporated faster than DMAc, phase separation between PDMS and PVDF happened, as shown in Figure 3. With increasing exposure time, more and more THF evaporated, so on the top surfaces, white markings appeared, and the number increased.

### Crystalline Structure

The effect of the exposure time on the crystallinity of the PDMS–PVDF membranes was investigated. As illustrated in Figure 3, the PDMS–PVDF membranes exhibited strong peaks at about 17.5, 20.5, and 27.5°; this was attributed to the typical crystalline peaks of PVDF.[35] However, when the exposure time was longer than 50 s, there appeared a new peak around 10.5–15.6°, which was assigned to the PDMS amorphous peak.[37] The intensity of the peak increased with increasing exposure time. This indicated that when the exposure time reached a certain value, the phase separation between PDMS and PVDF occurred because of the excessive evaporated THF. So, from Figure 2(d), we observed that there were lots of PDMS white markings on the top surfaces of the membranes; this could have resulted in bad pore structure and poor mechanical properties of the membranes and could have further deteriorated the membrane VMD performances.

**Table III.** Characterization of PDMS–PVDF Membranes with Different Exposure Times

| Membrane | Porosity (%) | Mean pore radius (μm) | Membrane thickness (mm) |
|---|---|---|---|
| MT1 | 85.22 ± 3.25 | 0.39 ± 0.05 | 0.16 |
| MT2 | 83.62 ± 2.65 | 0.37 ± 0.04 | 0.20 |
| MT3 | 78.21 ± 2.33 | 0.35 ± 0.03 | 0.26 |
| MT4 | 76.72 ± 2.75 | 0.29 ± 0.05 | 0.28 |
| MT5 | 63.21 ± 3.05 | 0.18 ± 0.03 | 0.28 |
| MT6 | 59.44 ± 3.12 | 0.15 ± 0.03 | 0.28 |

**Table IV.** Water Contact Angles of PDMS–PVDF Membranes with Different Exposure Times

| Membrane | Contact angle of top surface (°) | Contact angle of bottom surface (°) |
|---|---|---|
| MT1 | 109.30 ± 2.23 | 131.45 ± 1.08 |
| MT2 | 99.81 ± 2.11 | 126.73 ± 1.23 |
| MT3 | 99.90 ± 1.03 | 120.03 ± 2.47 |
| MT4 | 100.41 ± 1.55 | 118.90 ± 2.16 |
| MT5 | 101.13 ± 1.37 | 116.48 ± 1.89 |
| MT6 | 102.60 ± 1.08 | 114.10 ± 2.05 |

### Membrane Pore Structure

In this study, the porosity, mean pore radius, and membrane thickness of MT1 to MT6 were measured, and the results are shown in Table III. With increasing exposure time, the porosity and mean pore radius of the PDMS–PVDF membranes decreased from 85.22 ± 3.01 to 59.33 ± 3.69% and from 0.39 ± 0.04 to 0.15 ± 0.03 μm, respectively; these were in accordance with the SEM measurements of the membrane morphology (Figure 2), in which the pore structure of the cross section changed from cellular to globule type. When the exposure time attained 50 s, phase separation resulted in quick decreases in the porosity and mean pore radius, according to the SEM and XRD analysis. The membrane thickness increased, and the MT4, MT5, and MT6 membranes had the same thickness. This could be explained in terms of the polymer concentration in the casting films as analyzed in the light transmittance measurement. With increasing exposure time, the polymer concentration in the casting film increased.

### Hydrophobicity

The hydrophobicity values of MT1 to MT6 were studied through water contact angle measurement, as illustrated in Table IV. With increasing exposure time, the water contact angle of the top surfaces first decreased quickly and then increased warmly; the water contact angle of the bottom surfaces decreased linearly. This can be explained from the point of the morphology of the membrane surfaces. According to Li *et al.*,[38] the pores on the membrane surface had an obvious effect on the water contact angle, and the hydrophobicity of the microporous membrane were improved with the increase in the surface porosity. As shown in Figure 2(d,e), it was obvious that as the exposure time increased, the surface porosity on both the top surface and bottom surface decreased, and when the exposure time was higher than 30 s, no pores were observed on the top surface at a magnification of 5000×. On the other hand, according to the XRD analysis, during a long exposure time, PDMS, which presented a rubbery state at ambient temperature, might have dissolved out from the blend polymer solution and existed in a rubbery state in the membrane; this could have caused an increase in the top membrane surface. As a result, MT1, obtained with the shortest exposure time, displayed the strongest hydrophobicity, and its water contact angles of the top

**Table V.** Mechanical Properties of PDMS–PVDF Membranes with Different Exposure Times

| Membrane | Young's modulus (MPa) | Tensile strength (MPa) | Elongation ratio (%) |
|---|---|---|---|
| MT1 | 11.01 ± 2.76 | 0.39 ± 0.16 | 22.53 ± 1.31 |
| MT2 | 48.06 ± 4.20 | 2.82 ± 0.15 | 92.90 ± 2.53 |
| MT3 | 32.91 ± 2.90 | 1.67 ± 0.18 | 89.81 ± 1.60 |
| MT4 | 22.19 ± 3.04 | 0.84 ± 0.15 | 39.76 ± 4.15 |
| MT5 | 17.69 ± 3.15 | 0.73 ± 0.13 | 32.05 ± 2.61 |
| MT6 | 15.93 ± 2.13 | 0.55 ± 0.12 | 15.47 ± 3.07 |

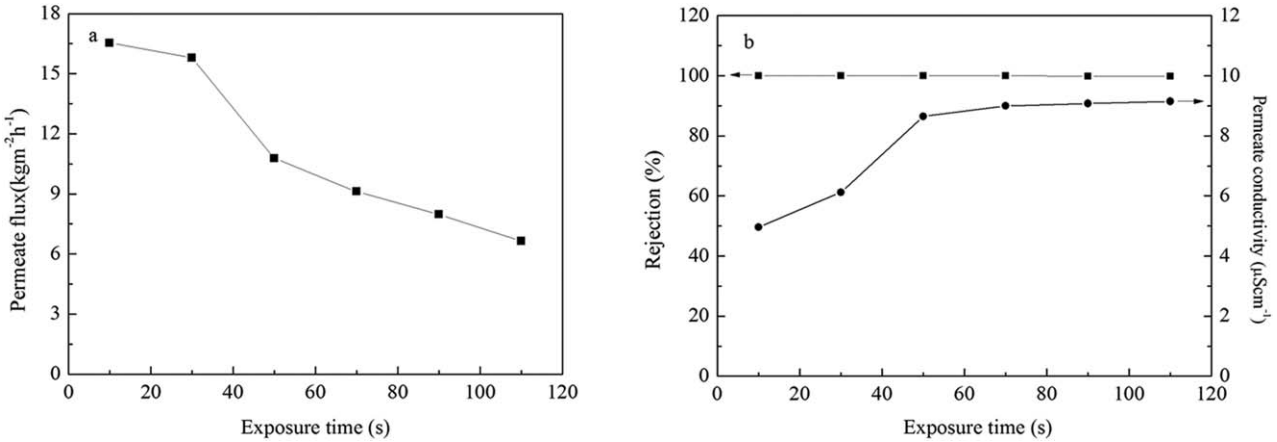


**Figure 4.** VMD performances of the PDMS–PVDF membranes with different exposure times: (a) flux and (b) rejection rates and permeate conductivity.

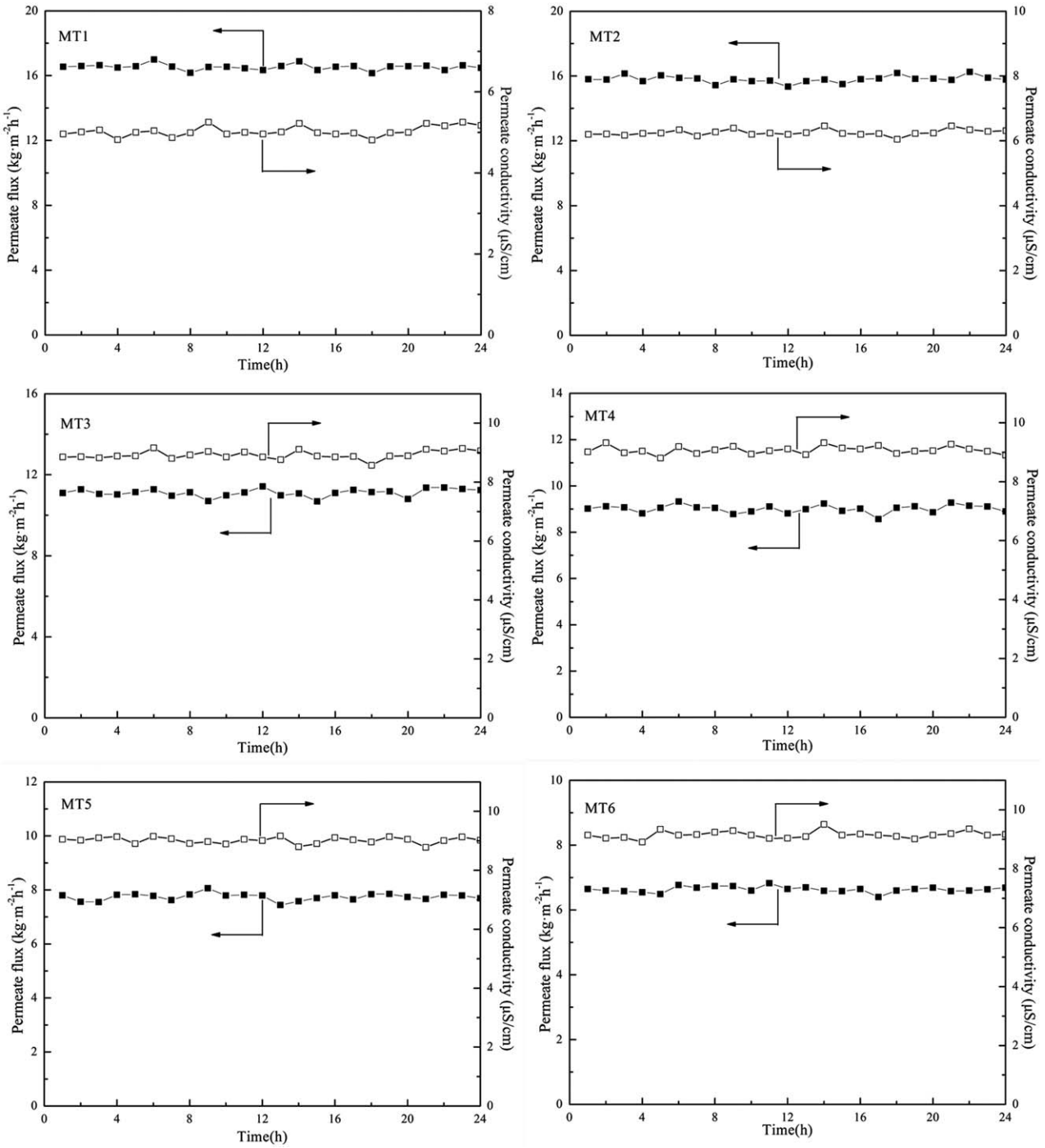


**Figure 5.** Long-term performance of the PDMS–PVDF membranes MT1–MT6 with a 20 g/L NaCl solution as the feed (vacuum = 90 kPa, feed temperature = 50 °C).

surface and bottom surface were 109.30 ± 2.23 and 131.45 ± 1.08, respectively.

### Mechanical Properties

As shown in Table V, the influence of the exposure time on the membrane mechanical properties of MT1 to MT6 were carried out. With increasing exposure time, the Young's modulus, tensile strength, and elongation ratio values of MT1 to MT6 first increased and then decreased. MT1 showed the worst mechanical properties, and MT2 exhibited the best mechanical properties in terms of Young's modulus, tensile strength, and elongation ratio, which were 48.06 ± 4.20 MPa, 2.82 ± 0.15 MPa, and 92.90 ± 2.53%, respectively. As analyzed for Figure 2(b), the cross-sectional SEM image of MT1 showed that there were lots of tearlike macropores on it; this could result in poor mechanical properties. A spongelike structure and a networklike microstructure were found on the cross section of MT2; this could have resulted in good mechanical properties. For MT3 to

MT6, according to the analysis of the morphology, the increase in the exposure time caused solid/liquid demixing; this resulted in the globule-type pore structure. With increasing exposure time, the diameter of the spherulitic microstructure grew, and the interspaces became larger and larger, as shown in Figure 2(c). This showed the worsening of the mechanical properties of the membranes.[24]

**VMD Performance**

The effects of the exposure time on the VMD performance of the PDMS–PVDF blend membranes for the 20 g/L NaCl aqueous solution at a feed temperature 50 °C and a permeate-side vacuum of 90 kPa are shown in Figure 4. With increasing exposure time from 10 to 110 s, the membrane permeate flux decreased from 16.54 to 6.65 kg $m^{-2} \cdot h^{-1}$. For all membranes (MT1 to MT6), the rejections to salt were higher than 99.9%. With increasing exposure time, as analyzed in the membrane pore structure, from MT1 to MT5, the membrane porosity and mean pore radius decreased; this caused a reduction in the membrane permeability.[24,25] Additionally, the increase in the membrane thickness (as shown in Table III) increased the transfer resistance of water molecules in the membrane, so we observed a rapid decline in the permeate flux. The results also show that the distillate conductivities of the PDMS–PVDF membranes increased from 4.96 to 9.15 μS/cm; this indicated that the salt rejection of MT1 to MT6 were higher than 99.9%. This suggests that there was no wetting during the VMD process for MT1 to MT6 because of its higher hydrophobicity, as shown in Table IV.

**Long-Term Performances**

To evaluate the stability of the PDMS–PVDF membrane for VMD, the PDMS–PVDF membranes (MT1–MT6) were tested for a 24 h continuous desalination with a 20 g/L NaCl aqueous at a feed temperature of 50 °C and a permeate-side vacuum of 90 kPa. To maintain a stable feed concentration, the permeated deionized water was returned to the feed tank. The dependence of the VMD performances, including the flux and permeate conductivity, on the operating time was reported in Figure 5. For all of the PDMS–PVDF (MT1–MT6) membranes, when the operating time was less than 24 h, the flux and permeate conductivity were stable; the rejections to salt were higher than 99.9% during the 24 h test. These results indicate that all of the PDMS–PVDF (MT1–MT6) membranes were of great potential for use in the VMD process.

## CONCLUSIONS

In this study, microporous PDMS–PVDF blend membranes were prepared via a NIPS process to investigate the effect of the exposure time on the membrane properties and VMD performance. The light transmittance of the casting solution, membrane morphology, pore structure, crystalline structure, hydrophobicity, and mechanical properties of the prepared membranes were measured. As the exposure time increased, the concentration of PVDF, PDMS, and additives on the membrane top surfaces increased gradually; this induced the crystallization of the PVDF polymer in the coagulation bath and caused the demixing to change from liquid/liquid to solid/liquid. So, we observed that with increasing exposure time, the precipitation rate of all of the casting solutions increased. All of the SEM images of the cross section showed a similar pore structure. A spongelike structure substrate layer with a thin realm of fingerlike structure existed under the top surface. The pore structure changed from the cellular type to globule type. Phase separation occurred between the PDMS polymer and PVDF polymer. The membrane porosity and mean pore radius of the PDMS–PVDF membranes decreased, and the membrane thickness increased. The water contact angle of the top surface first decreased quickly and then increased warmly, and the water contact angle of the bottom surface decreased linearly. The Young's modulus, tensile strength, and elongation ratio of MT1 to MT6 increased first and then decreased.

The VMD performances of the PDMS–PVDF blend membranes for the 20 g/L NaCl aqueous solution at a feed temperature of 50 °C and a permeate-side vacuum of 90 kPa were conducted. With increasing exposure time from 10 to 110 s, the membrane porosity and mean pore radius decreased, and the membrane thickness increased; this could reduce the membrane permeability. The salt rejection of MT1 to MT6 was higher than 99.9%; this suggested that there was no wetting during the VMD process for MT1 to MT6 because of its higher hydrophobicity.

## REFERENCES


1. Kang, G. D.; Cao, Y. M. *J. Membr. Sci.* **2014**, *463*, 145.
2. Drioli, E.; Ali, A.; Simone, S.; Macedonio, F.; Al-Jlil, S. A.; Al Shabonah, F. S.; Al-Romaih, H. S.; Al-Harbi, O.; Figoli, A.; Criscuoli, A. *Sep. Purif. Technol.* **2013**, *115*, 27.
3. Tong, D. Q.; Wang, X. Z.; Ali, M.; Lan, C. Q.; Wang, Y.; Drioli, E.; Wang, Z. H.; Cui, Z. L. *Sep. Purif. Technol.* **2016**, *157*, 1.
4. Zuo, J.; Bonyadi, S.; Chung, T. S. *J. Membr. Sci.* **2016**, *497*, 239.
5. Chen, K. K.; Xiao, C. F.; Huang, Q. L.; Liu, H.; Liu, H. L.; Wu, Y.; Liu, Z. *Desalination* **2015**, *375*, 24.
6. Lin, L.; Geng, H. X.; An, Y. X.; Li, P. L.; Chang, H. Y. *Desalination* **2015**, *367*, 145.
7. Kharraz, J. A.; Bilad, M. R.; Arafat, H. A. *J. Membr. Sci.* **2015**, *495*, 404.
8. Simone, S.; Figoli, A.; Criscuoli, A.; Carnevale, M. C.; Alfadul, S. M.; Al-Romaih, H. S.; Al. Shabouna, F. S.; Al-Harbi, O. A.; Drioli, E. *Desalination* **2014**, *344*, 28.
9. Devi, S.; Ray, P.; Singh, K.; Singh, P. S. *Desalination* **2014**, *346*, 9.
10. Shirazi, M. M. A.; Kargari, A.; Tabatabaei, M. *Chem. Eng. Process. Process Intensif.* **2014**, *76*, 16.
11. Fan, H. W.; Peng, Y. L.; Li, Z. H.; Chen, P.; Jiang, Q.; Wang, S. B. J. *Polym. Res.* **2013**, *20*, 134.
12. Sarbatly, R.; Chiam, C. K. *Appl. Energy* **2013**, *112*, 737.
13. Song, Z. W.; Jiang, L. Y. *Chem. Eng. Sci.* **2013**, *101*, 130.
14. Essalhi, M.; Khayet, M. *J. Membr. Sci.* **2013**, *433*, 167.
15. Edwie, F.; Teoh, M. M.; Chung, T. S. *Chem. Eng. Sci.* **2012**, *68*, 567.

16. Tang, Y. D.; Li, N.; Liu, A.; Ding, S. K.; Yi, C. H.; Liu, H. *Desalination* **2012**, *287*, 326.
17. Fan, H. W.; Peng, Y. L. *Chem. Eng. Sci.* **2012**, *79*, 94.
18. Singh, D.; Sirkar, K. K. *J. Membr. Sci.* **2012**, *389*, 380.
19. Prince, J. A. Prince; Singh, G.; Rana, D.; Matsuura, T.; Anbharasi, V.; Shanmugasundaram, T. S. *J. Membr. Sci.* **2012**, *387*, 80.
20. Wang, P.; Teoh, M. M.; Chung, T. S. *Water. Res.* **2011**, *45*, 5489.
21. Teoh, M. M.; Chung, T. S.; Yeo, Y. S. *Chem. Eng. J.* **2011**, *171*, 684.
22. Simone, S.; Figoli, A.; Criscuoli, A.; Carnevale, M. C.; Rosselli, A.; Drioli, E. *J. Membr. Sci.* **2010**, *364*, 219.
23. Thomas, R.; Guillen-Burrieza, E.; Arafat, H. A. *J. Membr. Sci.* **2014**, *452*, 470.
24. Peng, Y. L.; Fan, H. W.; Dong, Y. J.; Song, Y. N.; Han, H. *Appl. Surf. Sci.* **2012**, *258*, 7872.
25. Figoli, A.; Simone, S.; Criscuoli, A.; Al-Jlil, S. A.; Al Shabouna, F. S.; Al-Romaih, H. S.; Di Nicolò, E.; Al-Harbi, O. A.; Drioli, E. *Polymer* **2014**, *55*, 1296.
26. Hou, D.; Wang, J.; Sun, X. C.; Ji, Z. G.; Luan, Z. K. *J. Membr. Sci.* **2012**, *405*, 185.
27. Khayet, M.; Khulbe, K. C.; Matsuura, T. *J. Membr. Sci.* **2004**, *238*, 199.
28. Teoh, M. M.; Chung, T. S. *Sep. Purif. Technol.* **2009**, *66*, 229.
29. Lang, W. Z.; Zhang, X.; Shen, J. P.; Xu, H. P.; Xu, Z. L.; Guo, Y. J. *Desalination* **2014**, *341*, 72.
30. Zhang, X.; Lang, W. Z.; Xu, H. P.; Yan, X.; Guo, Y. J.; Chu, L. F. *J. Membr. Sci.* **2014**, *469*, 458.
31. Zhang, X.; Lang, W. Z.; Yan, X.; Lou, Z. Y.; Chen, X. F. J. *Membr. Sci.* **2016**, *499*, 179.
32. Xu, H. P.; Lang, W. Z.; Yan, X.; Zhang, X.; Guo, Y. J. J. *Membr. Sci.* **2014**, *467*, 142.
33. Wang, Z. Y.; Sun, L. Q.; Wang, Q.; Li, B. A.; Wang, S. C. *Eur. Polym. J.* **2014**, *60*, 262.
34. Chen, Z. L.; Rana, D.; Matsuura, T.; Yang, Y. F.; Lan, C. Q. *Sep. Purif. Technol.* **2014**, *133*, 303.
35. Sun, D.; Liu, M. Q.; Guo, J. H.; Zhang, J. Y.; Li, B. B.; Li, D. Y. *Desalination* **2015**, *370*, 63.
36. Essalhi, M.; Khayet, M. *J. Membr. Sci.* **2014**, *454*, 133.
37. Sun, D.; Li, B. B.; Xu, Z. L. *Desalination* **2013**, *322*, 159.
38. Li, Q.; Xu, Z. L.; Liu, M. *Adv. Technol.* **2011**, *22*, 520.